# Temporal dynamics of land use land cover (LULC) changes and assessment of environmental and climatic parameters using remote sensing and GIS: A case study in Limboti Reservoir, Loha Taluka, Maharashtra, India

K. Suresh Kumar Patro, Vinod Kumar Yadav\*, Waghmare Sneha Dadarao and Arpita Sharma

Fisheries Economics, Extension and Statistics Division (FEESD), ICAR-Central Institute of Fisheries Education, Mumbai - 400 061, Maharashtra, India



# Abstract

In this study, multispectral satellite data from Landsat 4-5 TM and Landsat 8 OLI/TIRS was used to analyse Land Use Land Cover (LULC) change detection and to retrieve environmental parameters. The LULC change detection was done between 2007 and 2021. This study used the supervised classification-maximum likelihood approach in ArcGIS 10.3 software to detect LULC in Loha Taluka, Maharashtra. The taluka was classified into four major LULC classes, viz. water, vegetation, settlement and barren-land. Changes in LULC directly or indirectly will also induce a change in the environmental parameters. Environmental parameters (water surface temperature, chlorophyll-a concentration and total suspended solids) were analysed for Limboti Reservoir. Data were predicted for next two years (2022 and 2023) using multiplicative seasonal decomposition and Holt-Winter's multiplicative method and trends of each parameter were analysed using Mann-Kendall trend method. For both years, vegetative land was the most extensive LC in Loha Taluka, accounting for more than 60% of the total land area. However, throughout these years, urbanisation was rampant and vegetative land was converted to settlement. In these years, open water resources such as reservoirs, lakes and rivers covered a very small percentage of the total area, which is a serious threat to the ecosystem. As a result, proper water body management is essential; otherwise, these resources will be destroyed and will no longer be able to contribute to the area's socioeconomic growth.



#### \*Correspondence e-mail: vinodkumar@cife.edu.in

#### Keywords:

Change detection, Chlorophyll content. Land use land cover, Water quality, Water surface temperature

> Received: 08.05.2023 Accepted: 06.09.2024

## Introduction

With large variations in precipitation, surface temperature and other climatic factors, global climate change has emerged as a serious danger to water resources (Bhadoriva et al., 2020). Climate change is expected to have an impact on the hydrology of most regions of the world by influencing temperature, rainfall, evapotranspiration (IPCC, 2007) and eventually runoff, as well as the planning characteristics (e.g., capacity) and performance (reliability, resilience, vulnerability and sustainability) of water resources infrastructures such as, reservoirs (Soundharajan et al., 2016).

These changes will impact interannual and seasonal streamflow variability (Li and Jin, 2017) leading to changes in regional water availability. The negative environmental and socio-political impacts of climate change will intensify, particularly in poor and developing countries including India (NAPCC, 2008; DARA, 2012). Increased water temperatures, decreasing dissolved oxygen levels and increased toxicity of contaminants are all expected to be prevalent effects of climate change on freshwater systems (Ficke et al., 2007). It may become extremely difficult to manage reservoirs to achieve conflicting and competing purposes optimally in the future due to uncertain water availability and demand (Bhadoriya et al., 2020). India is a country with many reservoirs, large, medium and small. These reservoirs were crucial in the development of India's culture and settlements in villages, towns and cities. They supply water for irrigation, bathing, washing, fisheries and other recreational activities and any impact on reservoirs is bound to impact Indian society significantly.

There are various roles of geospatial technologies for monitoring and assessing the climatic and environmental parameters and land use land cover (LULC) change detection. Geospatial systems include thematic mapping, the Global Positioning System (GPS), remote sensing (RS) and Geographic Information Systems (GIS) (USGS, 2000). Remote sensing is the process of collecting data and knowledge about a phenomenon or a region without coming into direct contact with it and is alternative to in situ observations (Zaidi, 2012). Recent advancements in remote sensing techniques have enabled the acquisition of water quality data at geographical and temporal resolutions that are beyond the capability of infrequent and point scale in situ measurements (Zaidi, 2012). GIS technology allows researchers to analyse and process large amounts of data at high speed and in less time and remote sensing systems provide uniform measurements with high-speed for large areas in the digital form (Tayari et al., 2015). Remote sensing has been used to classify and map land cover and land use changes with different techniques and data sets (Butt et al., 2015). Conventional methods for assessing and monitoring water quality need a lot of time, data and money, which is often out of reach for developing countries (Zaidi, 2012; Karunakaran et al., 2019). Using the geographic capabilities of RS and GIS techniques to address these difficulties is a cost-effective and quality research solution for large areas (Zaidi, 2012; Karunakaran et al., 2019). Most of the research has been on optically active factors like temperature, chlorophyll-a (chl-a) and total suspended solids. Chlorophyll-a is measured to detect the algal growth in a water body, as excessive algal growth can indicate the risk of eutrophication (Boucher et al., 2018).

Land cover relates to the physical aspects of the environment, including vegetation, settlements, water bodies, forests and agricultural areas. Land use on the other hand, describes how a settlement's territory is utilised by people, such as for housing or other human activities (Chaudhary et al., 2008). LULC has become a critical component in measuring and monitoring environmental changes as well as managing natural resources (Kaul and Sopan, 2012). Data from Earth sensing satellites has been increasingly important in mapping the Earth's features and infrastructures, managing natural resources and analysing environmental change in recent years (Zubair, 2006). Land use land cover change detection based on remote sensing data is an important source of information for various decision support systems. Data generated from the change detection in land use and land cover, aid land conservation, sustainable development and water resource management (Tewabe and Fentahun, 2020). Remote sensing and Geographic Information Systems (GIS) are powerful and cost-effective methods for analysing the spatial and temporal change of LULC.

Remote sensing and GIS are critical tools for determining the factors driving LULC changes as well as understanding their relationship with the water quality of lakes and reservoirs (Fukushima *et al.*, 2007; Wei *et al.*, 2020). Because of their time and cost-effectiveness

over broad areas as well as remote sites, these techniques make monitoring and analysis of LULC change and eutrophication more efficient than ground-based observations. In this regard, the Landsat Program, which consists of a succession of satellite missions, has the potential to monitor and quantify reservoir water quality parameters and LULC change at a scale that allows natural and human-induced causes to be distinguished (Gómez et al., 2016), due to its extensive history and reasonably high spatial resolution.

## Progress in water quality monitoring

Application of remote sensing and research in water quality monitoring have progressed from the early stages of identifying water quality indicators to remote monitoring, mapping and forecasting. The spectral features of the waterbody are determined mainly by the water body's material composition and a variety of water conditions. The key factors that affect water quality include suspended particles in water (turbidity), algae (Chlorophyll, Carotenoids), chemicals (nutrients, insecticides, metals), dissolved organic matter, heat emissions, pathogens and oil compounds (Fengyun, 2010). Water surface temperature, sea surface temperature, total dissolved solids, total suspended solids, water transparency. Chlorophyll a concentration, dissolved organic matter. the vertical attenuation coefficient of water incident and outgoing light and some integrated pollution indexes such as nutritional status index are all water quality parameters that can be monitored using remote sensing (Hendrata and Umbro, 2019; Adjovu et al., 2023). Overall, in the use of remote sensing techniques for monitoring water quality, extracting the concentrations of suspended matter in water and chlorophyll represents a more advanced technology.

# Existing problems in water quality monitoring

Remote sensing and GIS are two new technologies for monitoring water quality. On various spatial and temporal scales, remote sensing can offer the essential information for quantifying and analysing water properties and landscape features. It offers exciting opportunities to investigate fluvial patterns and processes by utilising wavelengths invisible to the naked eye, such as variations in infrared light reflected by different vegetation species. Although there has been significant improvement in water quality studies using remote sensing technologies, there are still several issues such as: (1) The ideal spectral resolution, time resolution, and geographical resolution for water quality monitoring are still unknown for water quality remote sensing; (2) Monitoring accuracy is low, and present techniques are almost empirical and semi-empirical in nature; (3) Existing algorithms are partial, localised and seasonal, as well as having limited applicability and adaptability; (4) Water quality can be evaluated via remote sensing technology, with floating sediment, chlorophyll, clarity, turbidity, and other metrics being the most common and (5) As the band utilised in water quality monitoring is very sluggish and concentrated mainly in the visible and near-infrared ranges, microwave and hyperspectral remote sensing data are less commonly used in water quality quantitative remote sensing inversion applied research.

The primary aim of this study was to use GIS and remote sensing techniques to determine the extent of LULC changes in the Loha Taluka, Maharashtra, India, over 14 years and to analyse the temporal variations in the environmental parameters of Limboti

Reservoir. The specific aims included distinguishing and delineating different LULC categories in Loha Taluka from 2007 to 2021; determining the shift in LULC classes through LULC mapping and change detection; retrieving all water quality parameters using RS and GIS techniques and analysing the temporal variation of trend and pattern of environmental as well as climatic parameters.

# Materials and methods

# Study area

The study region is located in the western portion of Nanded District, Maharashtra, India (Fig. 1). The Limboti Reservoir, located in Limboti Village of Loha Taluka (18.947388°N; 77.115440°E), Nanded District, is a small reservoir constructed on the Manyad River, completed in 2007. This reservoir lies near the border of Nanded and the Latur districts (Hussain *et al.*, 2012), with the major part of the reservoir situated in Nanded District. The temperature ranges typically from 14 to 43°C throughout the year, with temperatures rarely falling below 10.5°C or rising over 45°C. From 29 March to 01 June, it is hot season, with an average daily high temperature of over 40°C. May is the hottest month in Nanded, with average highs of 42.2°C and lows of 27.2°C. From 05 July to

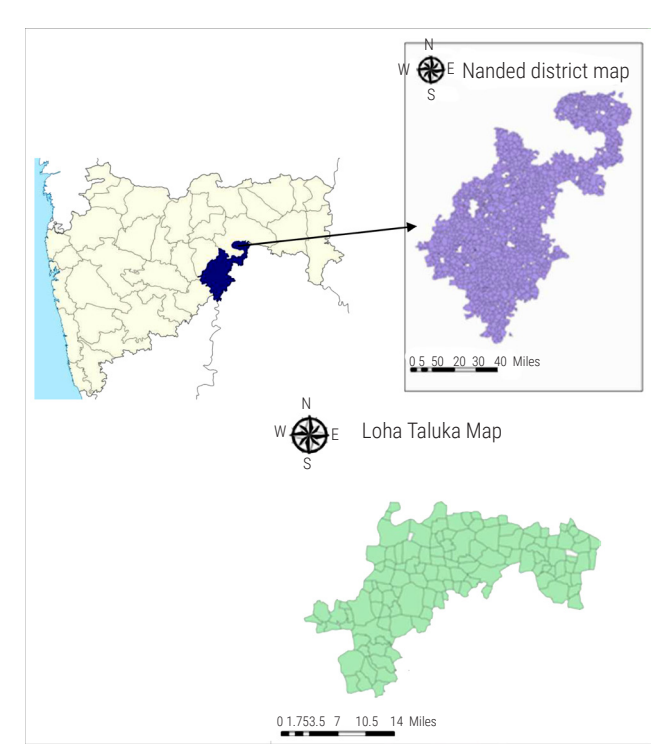


Fig. 1. Map of the study area

Table 1. Data sources

	Data	Date	Bands/colour	Source
Data for LULC analysis	Landsat 4-5 TM	27-09-2007	Multispectral	USGS- Earth Explorer
	Landsat 8 OLI/TIRS C1 Level-1	12-05-2021	Multispectral	USGS- Earth Explorer
Data for retrieval of environmental parameters	Landsat 8 OLI/TIRS C1 Level-1	2013 to 2021	Multispectral	USGS- Earth Explorer
Climatic parameters	MMAX temperature, MMIN temperature, TMRF, MWS			Indian Meteorological Department

26 January, it is cold season, with an average daily high temperature of less than 32.8°C. December is the coldest month in Nanded, with an average low of 14°C and high of 30°C. The rainy season starts around 27 May and lasts for 4.3 months, ending around 04 October. In Nanded, the cloudiest month of the year is July, when the sky is overcast or mostly cloudy during 89% of the time.

#### Data collection

Satellite images were used for the land use/land cover LULC and environmental parameter analysis. Landsat 8 OLI/TIRS and Landsat 4-5 TM satellites were selected for this purpose. Images were selected, downloaded and retrieved from the United States Geological Survey-Earth Explorer (https://earthexplorer.usgs. gov/). In particular, Landsat images have been very helpful in the larger-scale classification of various landscape components (Ozesmi and Bauer, 2002). Many of the current studies have been built from data retrieved by the Landsat satellite series, which has produced an extensive record of earth observation spanning more than 40 years (Flood, 2017). For the LULC study, two images were collected, one from Landsat 4-5 TM and one from Landsat 8 OLI/TIRS. Both the images were Tier-1, Level-1 data from USGS's repository. Multispectral images from 2013 to 2021 were used for environmental parameter retrieval. For the analysis of climatic parameters, data of the Nanded District were collected from 1975 to 2021 from the Indian Meteorological Department (IMD). The details of the images and data are shown in Table 1.

In addition to Loha Taluka, other regions were visible in the Landsat images obtained from the USGS. The images were clipped using ArcGIS Pro using a shapefile to extract the study region. Fig. 2 shows the shapefile overlaid on the Landsat image for 2021 while Fig. 3 displays the study area for the year 2021 after clipping.

# Methodology

# LULC classification and change detection

# Image pre-processing and classification

Prior to the identification of change, satellite image pre-processing is critical, with the primary goal of building a more direct link between the recorded data and biophysical phenomena (Coppin et al., 2004). The stages of image pre-processing are: detection and restoration of bad lines, geometric rectification or co-registration, absolute methods such as atmospheric and radiometric calibration, comparative methods such as topographic correction for rugged terrain and cloud masking if necessary. All satellite data were analysed by assigning per-pixel signatures and categorising the study area into four classes based on the Digital Number (DN) value of various landscape characteristics. Bands 1, 2, 3, 4, 5 and 7 and

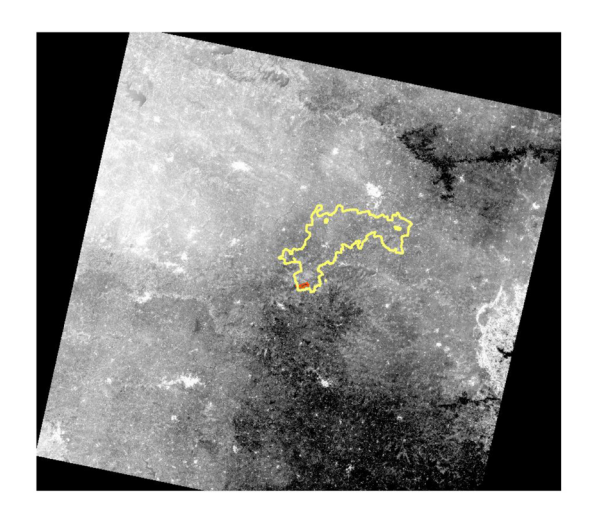


Fig. 2. Extracting study area from Landsat image *i.e.*, Limboti Reservoir (red) and Loha taluka (yellow)

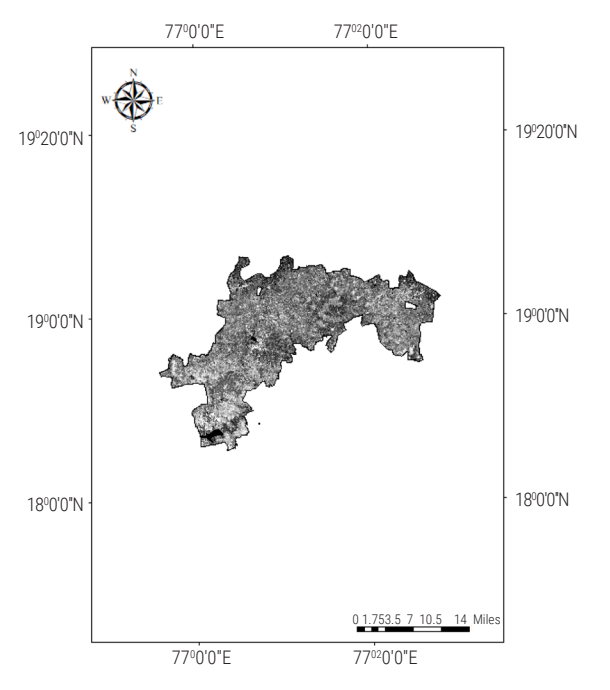


Fig. 3. Area of interest after clipping

2, 3, 4, 5, 6 and 7, which correspond to all visible and infrared bands for Landsat-5TM and Landsat-8 (OLI), respectively, were combined for classification using a pixel-based supervised classification algorithm after pre-processing.

Fig. 4 represents the composite band for bands 1 to 7 for Loha Taluka, 2021 and the colour infrared (vegetation) band combination was used to classify all classes. The classifier was trained by drawing 255 polygons for the year 2007 and 286 for 2021. To classify the images based on their spectral characteristics, Maximum likelihood classifier (MLC) was used. The delineated classes were water bodies, vegetation, settlements and barren land (Table 2).

Table 2. Classes delineated on the basis of supervised classification

Class name	Description
Water body	River, open water, lakes, ponds and reservoirs
Vegetation	Crop fields, forests and mixed forest lands
Settlement	Residential, commercial, industrial, transportation, roads, mixed urban
Barren land	Barren area with no vegetation

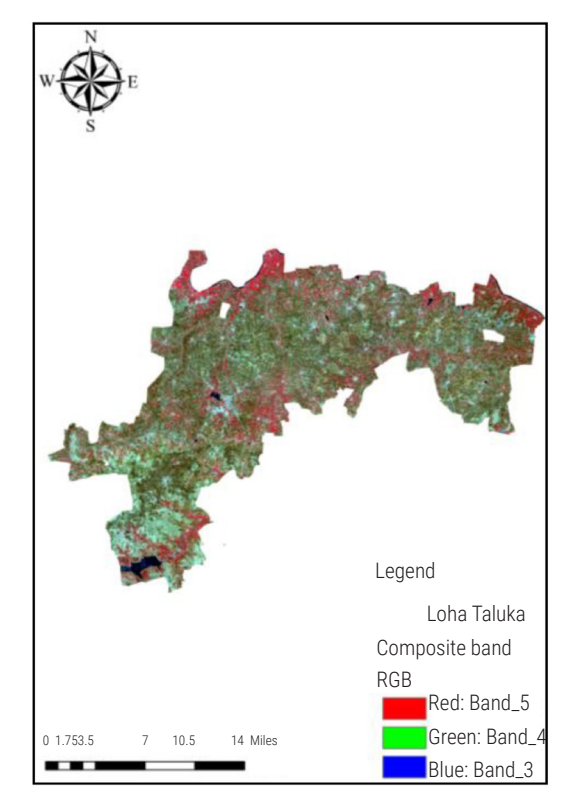


Fig. 4. Colour Infrared (Vegetation) band combination

### LULC change detection

The study used ArcGIS 10.3 to execute a post-classification change detection approach. The overlay method was used to acquire changes in land cover/land use throughout the selected time period. The implementation of this approach yielded a two-way cross-matrix, which was utilised to describe the primary forms of change in the research area. Cross-tabulation analysis on a pixel-by-pixel basis was used to determine the number of conversions from one land cover category to another, as well as their related area, across the evaluated time. As a result, these two classified maps yielded a new thematic layer with various combinations of "from-to" shift classes.

# Retrieval of environmental parameters (Chl-a, WST and TSS)

Chlorophyll-a concentration is a well-known indicator of ecological health of an aquatic environment and it has long been used to assess water quality and trophic condition. Satellite remote sensing is a strong instrument for monitoring and managing water quality that

has the advantages of being cost-effective, time-efficient, offering synoptic coverage and having a relatively high temporal resolution (Le *et al.*, 2013). Retrieval of Chl-a from the satellite sensors over the study region involves four steps *viz.*, (1) Obtaining absolute TOA Reflectance from scaled DN values in the case of Landsat-8 OLI, (2) Conversion of TOA Reflectance to SURFACE REFlectance, (3) Conversion of the Surface Reflectance to corresponding Remote Sensing Reflectance (Rrs) at these bands and finally (4) Retrieval of the water quality parameters from Rrs utilising the proposed empirical multivariate regression model (EMRM). The model used for the assessment of Chlorophyll-a concentration from satellite images is based on Zhou *et al.* (2020).

## **DN** to Radiance

Each pixel has a numerical value known as a digital number (DN) that records the strength of electromagnetic energy. Radiance is the radiant flux that a particular surface emits, reflects, transmits, or receives per unit solid angle per unit projected area.

#### Gain and bias method

DN to radiance conversion formula utilising gain and bias values is:  $L_x = gain \times DN + Bias$ 

 ${\rm L}_{\lambda}$  is the cell value as radiance; DN is the cell value digital number; gain is the gain value for a specific band; Bias is the bias value for a particular band.

## Spectral radiance scaling method

The formula used in this process is as follows:

$$L_{\lambda} = \left(\frac{LMAX_{\lambda} - LMIN_{\lambda}}{QCALMAX - QCALMIN}\right) \times (QCAL - QCALMIN) + LMIN_{\lambda}$$

 $L_{\lambda}$  is the cell value as radiance; QCAL is digital number; LMIN $_{\lambda}$  is spectral radiance scales to QCALMIN; LMAX $_{\lambda}$  is spectral radiance scales to QCALMAX; QCALMIN is the minimum quantised calibrated pixel value (typically = 1); QCALMAX is the maximum quantised calibrated pixel value (usually = 255)

#### Radiance to ToA Reflectance

$$P_{\lambda} = \frac{\pi \times L_{\lambda} \times d^{2}}{ESUN_{\lambda} \times \cos \theta_{c}}$$

 $P_{\lambda}$  = Unitless planetary reflectance;  $L_{\lambda}$  = spectral radiance (from earlier step); d = Earth-Sun distance in astronomical units; ESUN<sub> $\lambda$ </sub> = mean solar exoatmospheric irradiances;  $\theta_{s}$  = solar zenith angle.

**Processing:** Processing of the imagery was done using ESA-SNAP software.

**ESA-SNAP:** All Sentinel Toolboxes use the Sentinel Application Platform (SNAP), a shared software program designed for seamless data processing. The following technological breakthroughs make SNAP well suited for Earth observation (EO) processing and analysis: extensibility, portability, a modular rich client platform, tiled memory management, and a graph processing architecture. In addition to supporting Sentinel sensors, SNAP and the individual

Sentinel Toolboxes also accommodate a variety of other sensor types.

Water surface temperature is a significant driver in ecology, biodiversity and species distribution and it is an essential variable for understanding the Earth's climate. Water surface temperature (WST) satellite remote sensing has many applications in aquatic ecological research. Retrieval of WST from the satellite sensors over the study region involves eight step viz., calculation of (1) Reflectance value (Ref); (2) MNDWI; (3) ToA (Top of Atmospheric) spectral radiance; (4) ToA to Brightness Temperature conversion (BT); (5) Proportion of vegetation  $P_{v}$ ; (6) Emissivity ( $\epsilon$ ); (7) combining both BT<sub>10</sub> and BT<sub>11</sub>, using the cell statistics tool and (8) water surface temperature (Vanhellemont 2020; Dadarao  $et\ al.$ , 2023).

### Reflectance value

ML is Band specific multiplicative rescaling factor from the metadata (REFLECTANCE\_MULT\_BAND\_x, where x is the band number); *Qcal* is quantised calibrated pixel value, corresponds to extracted band using extract by mask in ArcMap; AL is band-specific additive rescaling factor from the metadata (REFLECTANCE\_ADD\_BAND\_x, where x is the band number).

#### MNDWI

$$MNDWI = \frac{(Green - SWIR)}{(Green + SWIR)}$$

Green is band 3 (Visible green); SWIR is band 6 (Short wave infrared); MNDWI (The Modified Normalised Difference Water Index) uses green and SWIR bands for the enhancement of open water features. It also decreases built-up area features that are often correlated with open water in other indices.

# ToA (Top of Atmospheric) spectral radiance

ToA = ML x Qcal + AL

## ToA to Brightness Temperature conversion (BT)

BT = 
$$\left[\frac{K_2}{[\ln(k_1/L) + 1]}\right]$$
 - 273.15

K1 is Band-specific thermal conversion constant from the metadata (K1\_CONSTANT\_BAND\_x, where x is the thermal band number); is Band-specific thermal conversion constant from the metadata (K2\_CONSTANT\_BAND\_x, where x is the thermal band number); L is ToA. The radiant temperature is changed by adding absolute zero (about -273.15°C) to get the data in Celsius.

# Proportion of vegetation P

$$P_v = Square \left[ \frac{MNDWI - MNDWI_{min}}{MNDWI_{max} - MNDWI_{min}} \right]$$

Usually, the maximum and minimum values of MNDWI image can be displayed directly within the image itself in softwares such as ArcGIS, QGIS, ENVI and Erdas Imagine. If this option is not available, these values can be accessed by opening the properties of the raster layer.

## Emissivity (ε)

 $\varepsilon = 0.004 \times P_{y} + 0.986$ 

# Water Surface Temperature (WST)

WST = 
$$\begin{bmatrix} & BT \\ \hline 1 + \left(\frac{0.00115 \text{ X BT}}{1.4388}\right) \text{x In}(\varepsilon) \end{bmatrix}$$

# Total suspended solids (TSS)

Total suspended solids (TSS) are essential carriers of organic matter like nitrogen and phosphorus and their movement and migration are crucial to the global material cycling and change process (Bianchi and Allison, 2009). TSS directly influences the primary productivity of the water body by regulating the distribution of dispersed light in the water body (Zhang *et al.*, 2014), which affects the transparency and oxygen content of the water body and plays a key role in the aquatic ecological environment. To retrieve TSS concentration, the reflectance value of bands 3 and 4 is used, and the methods to find reflectance value are the same as for WST.

TSS = 172.191x 
$$\ln^2(\frac{R_3}{R_4})$$
-190.809  $\ln(\frac{R_3}{R_4})$  + 61.6 (Dadarao et al., 2023)

# Trendline prediction of environmental parameters

#### Mann-Kendall Trend test

The correlation between a time series' ranks and its chronological order serves as the foundation for the Mann-Kendall trend test (Mann, 1945; Kendall, 1975). When determining if a time series has a monotonic upward or downward trend, the Mann-Kendall test is used. The absence of a trend is the null hypothesis for this test; the alternative hypothesis, for the two-sided test, is that there is a trend, and for the one-sided test, that trend is upward (or downward). The MK Test employs the subsequent statistic for the time series:

$$S = \sum_{i=1}^{n-1} \sum_{j=k+1}^{n} sign(x_{j} - x_{k})$$

where; sign 
$$(x_j - x_k) = \begin{cases} 1 & \text{if } x_j - x_i > 0 \\ 0 & \text{if } x_j - x_i = 0 \\ -1 & \text{if } x_j - x_i < 0 \end{cases}$$

Normalised test statistics Z is computed as:

$$Z = \begin{cases} \frac{S-1}{\sqrt{VAS(S)}} & \text{if } S > 0\\ 0 & \text{if } S = 0\\ \frac{S+1}{\sqrt{VAS(S)}} & \text{if } S < 0 \end{cases}$$

The null hypothesis of no trend is rejected at p=0.01 if |Z|>2.575 and at p=0.05, if |Z|>1.96.

It is worth noting that if S > 0, later observations in the time series tend to be larger than those appearing earlier in the time series, and if S < 0, the opposite is true. While a low negative value of S suggests a declining tendency, a large positive value of S indicates the opposite. If  $n \ge 10$ , S is considered generally distributed with variance as:

S = VAR (S) = 
$$\frac{1}{18}$$
 [n(n - 1) (2n + 5) -  $\sum_{p=1}^{q} t_p(t_p - 1)$  (2t<sub>p</sub> + 5)

where n = number of data points; q = number of tied groups and is the number data values in group p.

The Kendall's Tau for two sets of data can be determined as:

Tau = 
$$\frac{\text{(Number of concordant pairs - Numbers of discordant pairs)}}{\text{n (n - q)/2}}$$

The Tau value varies between -1 and +1 representing a strong negative association to a strong positive association between the data sets.

## Multiplicative seasonal decomposition

Time series forecasting methods are a class of methods that can be utilised for forecasting (Mbuli *et al.*, 2020). Pal and Yadav (2022) used to analyse a time series, the usual approach is to decompose it into three components as in the following: Trend, Seasonality and Irregular component.

The mathematical representation of the decomposition approach is:

where, Yt is the time series value (actual data) at period t; St is the seasonal component (index) at period t; Tt is the trend-cycle component at period t; Et is the irregular (remainder) component at period t.

# Moving average: Four-quarter moving average and centred moving average

Seasonal adjustment: For multiplicative decomposition, the seasonally adjusted data are computed by dividing the original observation by the seasonal component. Seasonal adjustment allows a reliable comparison of values at different points in time.

$$\frac{Y_t}{T_t} S_t \times E_t$$

Deseasonalising the data allows to quantify seasonality through seasonal indices. After deseasonalisation of the data, by applying linear regression to both the deseasonalised data and the total data points, the coefficients a and b can be determined.

# Holt-Winter's multiplicative model

By adding a seasonal equation to Holt's equations, Winters (1960) generalised Holt's (1957) linear technique. Based on the pattern

revealed by the time plot, it is either additive or multiplicative. Fitting both additive and multiplicative models is recommended, followed by selecting the optimal model based on model adequacy checks. Greater current values are given more weight by the model, while values from the distant past are given less weight. The additive model is defined as follows:

$$L_{t} = \alpha \, \frac{Yt}{S_{t-m}} + \left(1 - \alpha\right) \left(L_{t-1} + T_{t-1}\right) \label{eq:local_total_local}$$

$$T_{+} = \beta (T_{+} - L_{+-1}) + (1 - \beta) T_{+-1}$$

$$S_t = Y \frac{Yt}{L_t} + (1 - Y) S_{t-m}$$

$$F_{t+1} = (L_t + T_t) S_{t-m+1}$$

where  $0 \le \alpha \le 1, 0 \le \beta \le 1, 0 \le Y \le 1$ :  $\alpha$ ,  $\beta$ , Y are the smoothing parameters.

Lt is the smoothed level at time t, Tt is the change in the trend at the time t, St is the seasonal smooth at time t, Ft+1 is the forecasting within the dataset and m is the number of seasons per year.

# **Results and discussion**

# LULC classification and change detection

The classified LULC map of Loha Taluka for the years 2007 and 2021 is given in Fig. 5. The statistics for classification, indicating the percentage cover and total area in hectares, are tabulated in Table 3. The land cover/land use practices observed in the taluka region between 2007 and 2021 are shown as a percentage of classes based on these results. The results show that a significant decline with respect to area coverage in Loha Taluka was observed in the barren land class. In contrast, the area of vegetation, water body and settlement classes had increased (Fig. 6). There has been a significant rise in water bodies (161.3%) and a significant decrease

ettlement classes had increased (Fig. 6). There has been particle

concent rise in water bodies (161.3%) and a significant decrease

Legend
LULC\_2007
Name

Water body
Vegetation

in barren land (49.46%). The vegetation area increased from 66.81 to 80.22%. Vegetation occupies the highest land cover in both 2007 and 2021, which is likely more than half. Settlements accounted for 1.54% of the entire area, although this figure has since risen to 2.93%. Dhorde et al. (2012) worked on evaluation of LULC in Mula-Mutha Watershed, Pune and compared the LULC change between the year 1989 and 2008 and found that there was a huge positive change in settlement, vegetation and agricultural land and water body while negative change in barren land. Masroor et al.(2022) worked on the influence of LULC alteration on climate variability in Aurangabad District and they compared the LULC change from 1999 to 2019 and found that there was a positive change for the areas of water body, settlement and barren land but a negative change in the area of agricultural land.

The comparison of each class from 2007 to 2021 revealed that there has been a significant change in land use and land cover over the 14 years. Table 4 shows that the total area of Nanded District changed from 2007 to 2021 is 84708.80 ha. The change from barren land to vegetation area in Nanded between 2007 and 2021 is significant, that include 18173.93 ha. Settlement area expanded from 1308.01 to 2485.25 ha between 2007 and 2021, with most of the increase coming from vegetation area; from which we can conclude that the conversion of forest and agricultural land boosted dwelling, road and industrial areas. In 2021, 5791.14 ha of vegetation land were changed to barren land and many agricultural lands were converted to unfertile and plotting areas. Due to growing urbanisation, 1114.34 ha of vegetative land were converted to settlement class

# Environmental and climatic parameters of Limboti Reservoir

Landsat-8 multispectral pictures were used to analyse the environmental parameters of Limboti Reservoir chlorophyll-a concentration, water surface temperature and total suspended particles. For each month from 2013 to 2021, data was collected

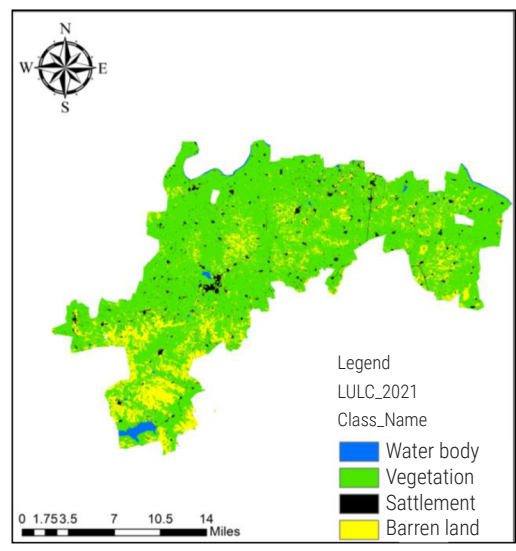


Fig. 5. Classified LULC map of Loha Taluka; for 2007 (left) and 2021 (right)

0 1.753.5

Sattlement

Barren land

Table 3. Land Use Land Covers Classes for Loha Taluka, Maharashtra

Landaniantina	20	2007		21	0/ 0/	
Land cover types	Area (Ha)	%	Area (Ha)	%	% Unange	% Change
Water body	341.16	0.04	891.46	1.05	+161.3	
Vegetation	56654.07	66.81	68021.8	80.22	+20.06	
Settlement	1309.26	1.54	2487.91	2.93	+90.02	
Barren land	26490.28	31.24	13386.62	15.79	-49.46	
Total	84794.77	99.99	84787.79	99.99		

Table 4. Relative change in area (ha) of land cover types between 2007 and 2021

		2021					
		Water body	Vegetation	Settlement	Barren land	Total	
2007	Water body	221.08	102.36	16.56	0.98	340.98	
	Vegetation	653.36	49043.95	1114.34	5791.14	56602.79	
	Settlement	8.24	646.55	546.67	106.55	1308.01	
	Barren land	5.05	18173.93	807.68	7470.34	26457.01	
	Total	887.73	67966.79	2485.25	13369.02	84708.80	

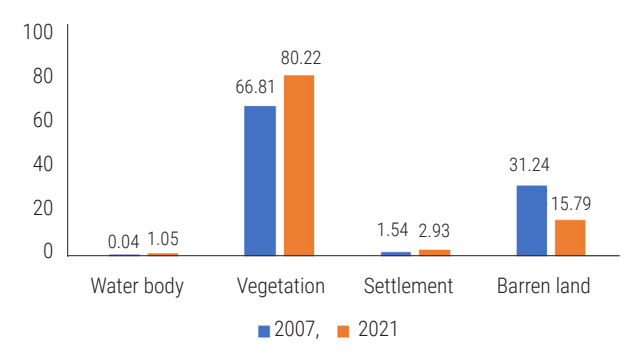


Fig. 6. Class-wise percentage land cover

season-wise: winter (January, February); pre-monsoon (March, April, May); monsoon (June, July, August, September) and post-monsoon (October, November, December) (October, November, December). The average of the collected data was used to determine the average value for the particular season.

The seasonal values of Chl-a, WST and TSS from 2013 to 2021 are shown in Fig. 7, chlorophyll-a value was highest (23.72 mg.m $^{-3}$ ) in monsoon in 2020 and lowest (2.21 mg.m $^{-3}$ ) in post-monsoon 2019; water surface temperature was highest (27.45 $^{\circ}$  C) in pre-monsoon in 2019 and lowest (19.71 $^{\circ}$ C) in winter in 2018 and total suspended solid concentration was highest (54.24 mg l $^{-1}$ ) in monsoon in 2021 and lowest (33.26 mg l $^{-1}$ ) in post-monsoon in 2013.

Table 5 shows the average water quality parameter changes from 2013 to 2021. It can be seen that the chl-a concentration increased from 2013 to 2021 in all seasons except post-monsoon, where we can clearly see a drastic decrease of about 31%; winter shows a hike of 39.57%, while pre-monsoon and monsoon show a 4.24 and 1.02% increase, respectively. In terms of water surface temperature, there is a definite upward trend in all four seasons, with the post-monsoon season having the most significant increase of 20.29%. There is a complete increase in total suspended solid concentration in all four seasons, with the most significant increase of 28.96% occurring in the monsoon season.

Fig. 8 shows the climatic parameters, *i.e.*, mean maximum temperature, mean minimum temperature and total mean rainfall,

Table 5. Average water quality parameter changes between 2013 to 2021

Seasons	Chlorophyll-a	Water Surface Temperature	Total Suspended Solids
Winter	+39.57	+2.35	+14.79
Pre-monsoon	+4.24	+2.96	+3.56
Monsoon	+1.02	+13.09	+28.96
Post-monsoon	-31.23	+20.29	+22.76

which were collected from IMD. Mean maximum temperature was highest (42.60°C) in pre-monsoon in 1978 and lowest (28.23°C) in monsoon 2007, likely mean minimum temperature was highest (32.5°C) in post-monsoon in 2007 and lowest (11.57°C) in post-monsoon in 1983 and total mean rainfall was highest (482.2 mm) in monsoon in 2013 and lowest (0 mm) in winter and post-monsoon seasons across multiple years.

In Limboti Reservoir, the total mean rainfall has no trend, indicating an inconsistent pattern in all four seasons. During the postmonsoon months, the mean maximum temperature increased, while during the pre-monsoon months, it decreased. In both the winter and post-monsoon months, the mean minimum temperature showed an increase. Table 6 presents a year-by-year trend analysis of climatic factors, demonstrating that mean maximum and minimum temperatures are increasing. In contrast, rainfall has no trend indicating an irregular rainfall pattern.

A correlation matrix with six components was built to know the relationship between environmental and climatic parameters (Fig. 9). From this it is evident that WST and Chl-a had a positive relationship. This is because when WST rises, it provides nutrients to the photic zones, which leads to greater photosynthesis (Bouffard et al., 2018). As fast water flow keeps particles suspended rather than allowing them to settle, there is a positive relationship between rainfall and TSS. Wind generates turbulence in the water, preventing solid particles from settling, according to a positive link between TSS and MWS. MMAX temperature and rainfall have a negative relationship, indicating that temperatures are high and rainfall is sparse during the pre-monsoon or summer seasons.

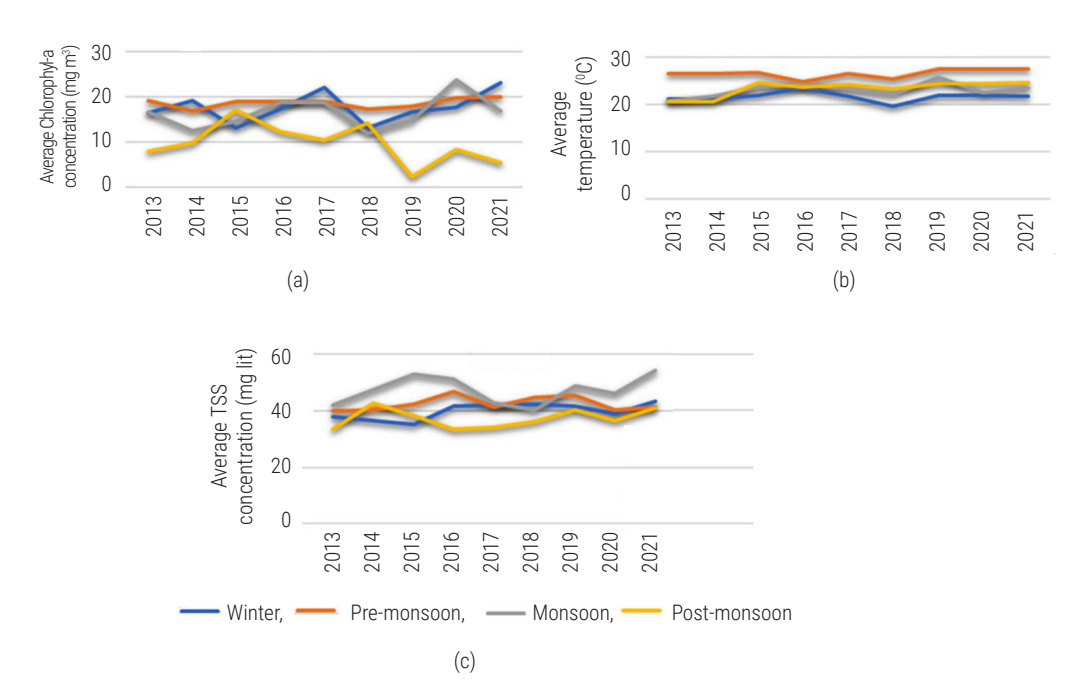


Fig. 7. Chart showing retrieved value of Chl-a, WST and TSS season wise from 2013-2021

Table 6. Trend analysis of climatic parameters during different seasons in Limboti Reservoir

Climatic parameters	Tau( au)	p-value	Remark
MMAX Temperature	0.225	0.028	Significant increasing trend
MMIN Temperature	1	< 0.0001	Significant increasing trend
Total Mean Rainfall	0.092	0.373	No trend

# Prediction of environmental parameters

The water quality metrics (Chl-a, WST and TSS) for the years 2022 and 2023 were predicted using the multiplicative seasonal decomposition model and Holt-Winter's multiplicative prediction

model. Table 7 and 8 shows the expected values for each of the three parameters by using both models for all four seasons for the year 2022 and 2023. The root mean square error is used as an indicator to determine which prediction model is superior for this data analysis (Table 9). Compared to Holt-Winter's multiplicative model, the multiplicative seasonal decomposition model had less inaccuracies. This is due to the presence of a seasonal factor in this model. Fig. 10 and 11 show the comparison graph for data between observed and predicted values for multiplicative seasonal decomposition and Holt-Winter's multiplicative model respectively; and from those figures, it is clear that there is significant variation between observed and predicted values in the case of

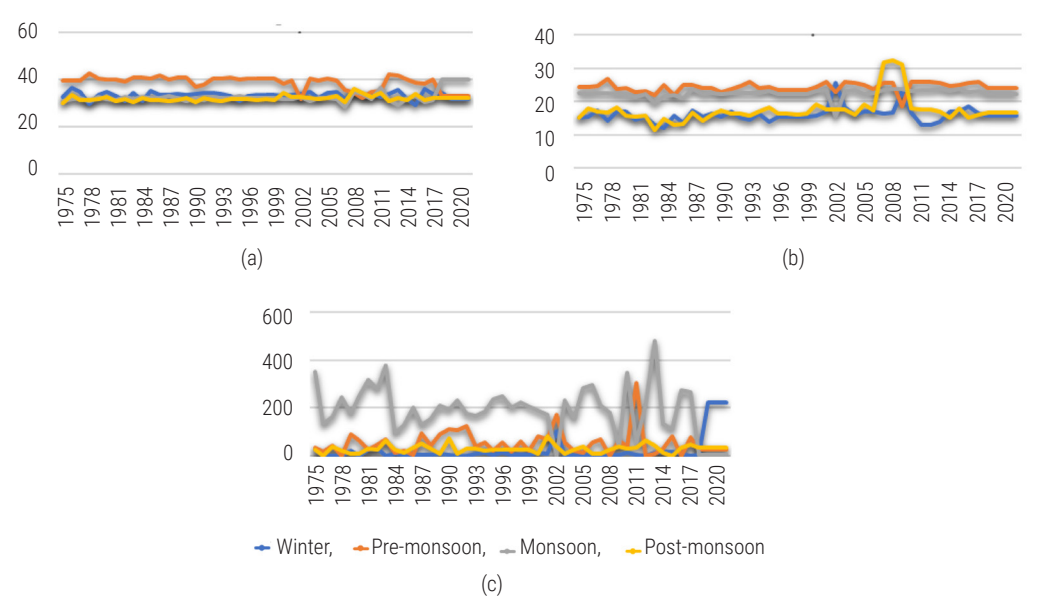


Fig. 8. Climatic parameters i.e., MMAX temperature (°C), MMIN temperature (°C) and Total mean rain fall (mm) of Limboti Reservoir between 1975-2021

Holt-Winter's multiplicative model compared to multiplicative seasonal decomposition method.

The results of the study through the application of GIS and remote sensing (RS) tools reveal that the land cover/land use practices in the study area have undergone significant changes over the 14 years period. The rise in the area of settlement and waterbody class (90 and 161.3%, respectively) and fall in the area of barren land (49.46%) was evidence of the LULC change in the study area. The fact that there has been an increase in vegetation area (20.02%) as barren lands were converted to vegetation land is surreal; we can assume that as the settlement grew, people began to engage in more agricultural activities. In the year 2021, there was a relatively small amount of water, accounting for only 1% of the entire area. As a result, the government and policymakers need to take the appropriate procedures and management methods to expand the taluka's water holding areas. These changes may have ramifications for long-term resource management and the well-being of local society. To avoid unfavourable LULC dynamics in the taluka. effective land management practices (soil and water conservation). enhanced agricultural inputs, integrated watershed management (land use planning and management) and active participation of the local population should be pursued. In this work, change detection analysis utilising GIS and remote sensing could provide vital information for planners and decision-makers to understand the patterns of land use dynamics, allowing for sustainable land management planning.

Water quality of the reservoir has deteriorated substantially as anthropogenic activities and industrial growth has increased. The

Table 7. Multiplicative Seasonal Decomposition model

Casaan	Parameters				
Season	Chl-a (mg.m <sup>-3</sup> )	WST (°C)	TSS (mg.l-1)		
Winter	17.14	21.38	43.14		
Pre-monsoon	18.16	25.45	45.57		
Monsoon	15.97	21.70	48.61		
Post-monsoon	9.87	22.32	40.46		
Winter	16.87	21.33	43.55		
Pre-monsoon	17.73	25.36	46.10		
Monsoon	15.94	21.63	49.77		
Post-monsoon	10.47	22.08	40.90		
	Pre-monsoon Monsoon Post-monsoon Winter Pre-monsoon Monsoon	Season         Chl-a (mg.m <sup>-3</sup> )           Winter         17.14           Pre-monsoon         18.16           Monsoon         15.97           Post-monsoon         9.87           Winter         16.87           Pre-monsoon         17.73           Monsoon         15.94	Season         Chl-a (mg.m³)         WST (°C)           Winter         17.14         21.38           Pre-monsoon         18.16         25.45           Monsoon         15.97         21.70           Post-monsoon         9.87         22.32           Winter         16.87         21.33           Pre-monsoon         17.73         25.36           Monsoon         15.94         21.63		

Table 8. Holt-Winters Multiplicative method

Coopen		Parameters				
2692011	Chl-a (mg.m <sup>-3</sup> )	WST (°C)	TSS (mg.l-1)			
Winter	18.52	20.17	44.60			
Pre-monsoon	20.08	24.02	47.52			
Monsoon	20.03	20.03	43.89			
Post-monsoon	20.97	20.97	40.25			
Winter	20.18	20.18	45.44			
Pre-monsoon	24.03	24.03	48.40			
Monsoon	20.04	20.04	44.68			
Post-monsoon	20.98	20.98	40.96			
	Pre-monsoon Monsoon Post-monsoon Winter Pre-monsoon Monsoon	Chl-a (mg.m³)           Winter         18.52           Pre-monsoon         20.08           Monsoon         20.03           Post-monsoon         20.97           Winter         20.18           Pre-monsoon         24.03           Monsoon         20.04	Season         Chl-a (mg.m³)         WST (°C)           Winter         18.52         20.17           Pre-monsoon         20.08         24.02           Monsoon         20.03         20.03           Post-monsoon         20.97         20.97           Winter         20.18         20.18           Pre-monsoon         24.03         24.03           Monsoon         20.04         20.04			

Table 9. Error comparison between both the models

Year	Model		Error		
		Chl-a	WST	TSS	
2022	Multiplicative Seasonal Decomposition	3.24	1.15	4.18	
	Holt-Winters Multiplicative method	10.29	5.95	8.34	
2023	Multiplicative Seasonal Decomposition	3.12	1.09	3.95	
	Holt-Winters Multiplicative method	9.68	5.60	7.85	

most effective, less expensive, and more reliable instruments for monitoring water quality parameters in various waterbodies (lakes, rivers and groundwater) include remote sensing and GIS. Environmental parameters (WST, Chl-a concentration and TSS) were retrieved and evaluated for a period of nine years, from 2013 to 2021 and predictions were made for the years 2022 and 2023. When compared to Holt-Winter's multiplicative model, multiplicative seasonality decomposition revealed less inaccuracy, implying that the presence of a seasonality factor in this data permitted multiplicative seasonal decomposition to be more accurate. Climate data such as MMAX temperature, MMIN temperature, and total mean rainfall were acquired from IMD and analysed to determine the trend from 1975 to 2021. The data revealed that the MMAX and MMIN temperatures are increasing and rainfall is unpredictable. Water quality has severely deteriorated as a result of increased human activity and industrial growth. By 2021, all the changes in land cover and land use patterns had a negative impact on water quality and accessibility, which could become a limiting factor in the future for both urban growth and agricultural practice, as well as  $cause \, further \, loss \, of \, already \, shrinking \, vegetation \, cover \, in \, watershed \,$ 

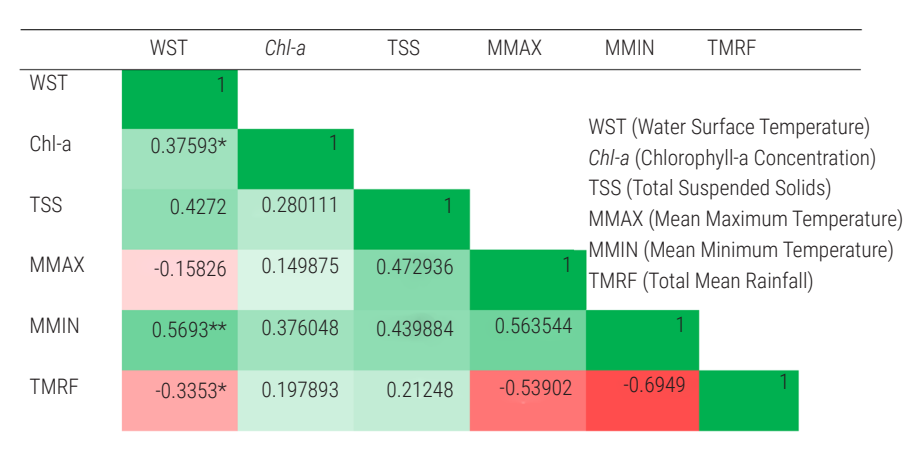


Fig. 9. Correlation Matrix

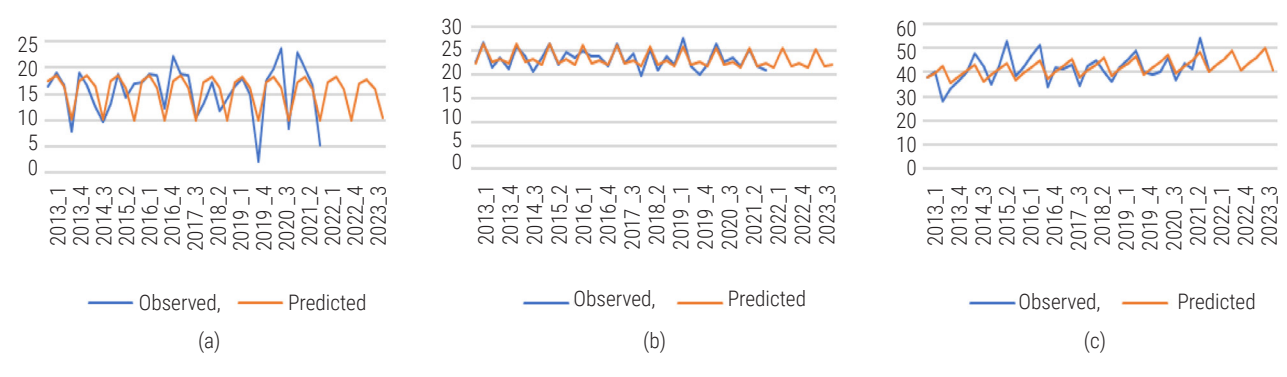


Fig. 10. Comparison between observed and predicted values of Multiplicative seasonal decomposition metho

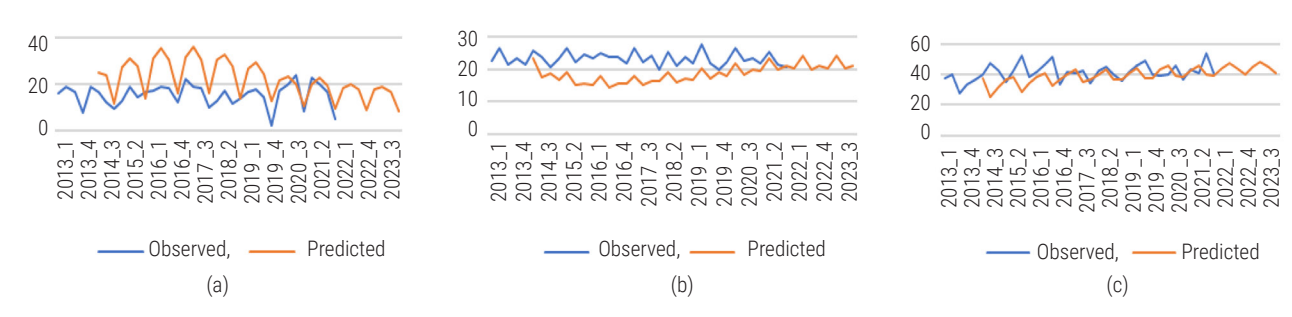


Fig. 11. Comparison between observed and predicted values of Holt-Winter's multiplicative model

areas. Land use and climate change scenarios have enhanced our understanding and visualisation of their potential impacts on the hydrology of the Limboti Reservoir. By utilising these scenarios, we can explore various land use and climate conditions to assess the reservoir's response. The research provides valuable insights for stakeholders and policymakers, enabling them to evaluate the effects of different strategies and to make more informed decisions for sustainable management.

## References

Adjovu, G. E., Stephen, H., James, D. and Ahmad, S. 2023. Measurement of total dissolved solids and total suspended solids in water systems: A review of the issues, conventional, and remote sensing techniques. *Remote Sens.*, 15(14): 3534.

Bhadoriya, U. P. S., Mishra, A., Singh, R. and Chatterjee, C. 2020. Implications of climate change on water storage and filling time of a multipurpose reservoir in India. *J. Hydrol.*, 590: 125542. https://doi.org/10.1016/j.jhydrol.2020.125542.

Bianchi, T. S. and Allison, M. A. 2009. Large-river delta-front estuaries as natural "recorders" of global environmental change. *Proc. Natl. Acad. Sci.*, 106(20): 8085-8092. https://doi.org/10.1073/pnas.0812878106.

Bonansea, M., Bazan, R., German, A., Ferral, A., Beltramone, G., Cossavella, A. and Pinotti, L. 2021. Assessing land use and land cover change in Los Molinos reservoir watershed and the effect on the reservoir water quality. J. S. Am. Earth Sci., 108: 103243. https://doi.org/10.1016/j.jsames.2021.103243.

Boucher, J., Weathers, K. C., Norouzi, H. and Steele, B. 2018. Assessing the effectiveness of Landsat 8 chlorophyll a retrieval algorithm for regional freshwater monitoring. *Ecol. Appl.*, 28(4): 1044-1054. https://doi.org/10.1002/eap.1708.

Butt, A., Shabbir, R., Ahmad, S. S. and Aziz, N. 2015. Land use change mapping and analysis using Remote Sensing and GIS: A case study of Simly watershed, Islamabad, Pakistan. *Egypt. J. Remote Sens. Space Sci.*, 18(2): 251-259.

Chaudhary, B. S., Saroha, G. P. and Yadav, M. 2008. Human induced land use/land cover changes in northern part of Gurgaon district, Haryana, India: natural resources census concept. *J. Hum. Ecol.*, 23(3): 243-252. https://doi.org/10.1080/09709274.2008.11906077.

Dadarao, W. S., Yadav, V. K., Patro, K. S. K., Meharoof, M. and Sharma, A. 2023. Temporal dynamics of LULC with environmental and climatic parameter assessment using remote sensing and GIS: A case study in Dimbe Reservoir, Ambegaon Taluk, Maharashtra, India: Use of remote sensing and GIS for LULC assessment. J. Inland Fish. Soc. India, 55(1): 75-93.

Dhorde, A., Das, S. and Dhorde, A. 2012. Evaluation of Land Use/Land Cover Change in Mula-Mutha Watershed, Pune Urban Agglomeration, Maharashtra, India, based on remote sensing data. *Earth Sci. India*, 5(3): 108-121.

Fengyun, M. 2010, March. Progress in water quality monitoring based on remote sensing and GIS. *IEEE*, 2: 208-211. https://doi.org/10.1109/CESCE.2010.246.

Ficke, A. D., Myrick, C. A. and Hansen, L. J. 2007. Potential impacts of global climate change on freshwater fisheries. *Rev. Fish Biol. Fish.*, 17(4): 581-613. https://doi.org/10.1007/s11160-007-9059-5.

Flood, N. 2017. Comparing Sentinel-2A and Landsat 7 and 8 using surface reflectance over Australia. *Remote Sens.*, 9(7): 659.

Fukushima, T., Takahashi, M., Matsushita, B. and Okanishi, Y. 2007. Land use/cover change and its drivers: A case in the watershed of Lake Kasumigaura, Japan. *Landsc. Ecol. Eng.*, 3(1): 21-31.

Gomez, C., White, J. C. and Wulder, M. A. 2016. Optical remotely sensed time series data for land cover classification: A review. *ISPRS J. Photogramm. Remote Sens.*, 116: 55-72. https://doi.org/10.1016/j.isprsjprs.2016.03.008.

- Hendrata, W. and Umbro, L. 2019. Analysis of sea surface temperature with total suspended solid algorithm based on satellite images data. In: *Proceedings of the International Seminar of Research month science and technology for people empowerment*, 23<sup>rd</sup> November 2018. Surabaya, Indonesia, p. 322-332.
- Hussaina, S., Maneb, V., Pradhanc, V. and Farooqui, M. 2012. Physico-chemical analysis of Limboti Dam water, Dist. Nanded, Maharashtra. J. Adv. Sci. Res., 3(01): 55-57.
- Karunakaran, D., Kumar Sahu, S., Pandit, A. and Sharma, A. P. 2019. Assessment of chlorophyll and water quality using remote sensing and GIS imagery in the Cauvery watershed of Karnataka, India. *Indian J. Fish.*, 66(2): 43-48.
- Kaul, H. A. and Sopan, I. 2012. Land use land cover classification and change detection using high resolution temporal satellite data. J. Environ., 1(4): 146-152.
- Li, Z. and Jin, J. 2017. Evaluating climate change impacts on streamflow variability based on a multisite multivariate GCM downscaling method in the Jing River of China. *Hydrol. Earth Syst. Sci.*, 21(11): 5531-5546. https://doi.org/10.5194/hess-21-5531-2017.
- Masroor, M., Avtar, R., Sajjad, H., Choudhari, P., Kulimushi, L. C., Khedher, K. M., Komolafe, A. A., Yunus, A. P. and Sahu, N. 2022. Assessing the influence of land use/land cover alteration on climate variability. An analysis in the Aurangabad District of Maharashtra State, India. *Sustainability*, 14(2): 642.
- Mbuli, N., Mathonsi, M., Seitshiro, M. and Pretorius, J. H. C. 2020. Decomposition forecasting methods: A review of applications in power systems. *Energy Rep.*, 6: 298-306.
- Ozesmi, S. L. and Bauer, M. E. 2002. Satellite remote sensing of wetlands. Wetl. Ecol. Manag., 10: 381-402.

- Soundharajan, B. S., Adeloye, A. J. and Remesan, R. 2016. Evaluating the variability in surface water reservoir planning characteristics during climate change impacts assessment. *J. Hydrol.*, 538: 625-639. https://doi.org/10.1016/i.jhydrol.2016.04.051.
- Tayari, E., Jamshid, A. R. and Goodarzi, H. R. 2015. Role of GPS and GIS in precision agriculture. *J. Sci. Res. Dev.*, 2(3): 157-162.
- Tewabe, D. and Fentahun, T. 2020. Assessing land use and land cover change detection using remote sensing in the Lake Tana Basin, Northwest Ethiopia. *Cogent Environ. Sci.*, 6(1): 1778998. https://doi.org/10.1080/2 3311843.2020.1778998.
- Vanhellemont, Q. 2020. Automated water surface temperature retrieval from Landsat 8/TIRS. *Remote Sensing of Environment*, 237: 111518.
- Wei, W., Gao, Y., Huang, J. and Gao, J. 2020. Exploring the effect of basin land degradation on lake and reservoir water quality in China. *J. Clean. Prod.*, 268: 122249. https://doi.org/10.1016/j.jclepro.2020.122249.
- Zaidi, A. Z. 2012. Water quality management using GIS and RS tools. In: Proceedings of the World Environmental and Water Resources Congress 2012: Crossing Boundaries, pp. 842-848.
- Zhang, Y., Wu, Z., Liu, M., He, J., Shi, K., Wang, M. and Yu, Z., 2014. Thermal structure and response to long-term climatic changes in Lake Qiandaohu, a deep subtropical reservoir in China. *Limnol. Oceanogr.*, 59(4): 1193-1202. https://doi.org/10.4319/lo.2014.59.4.1193.
- Zhou, X., Zhang, J., Chen, D., Huang, Y., Kong, W., Yuan, L., Ye, H. and Huang, W. 2020. Assessment of leaf chlorophyll content models for winter wheat using Landsat-8 multispectral remote sensing data. *Remote Sens.*, 12(16): 2574.
- Zubair, A. O. 2006. Change detection in land use and Land cover using remote sensing data and GIS: A case study of Ilorin and its environs in Kwara State. M. Sc. Dissertation University of Ibadan, Nigeria, pp. 1-54.